Journal of Beijing Institute of Technology, 2026, Vol. 35, No. 5

A Passive Synthetic Aperture Positioning Method for Sparse Radar Signal with Complex PRI

Huanhuan Li, Ran Tao✉

(School of Information and Electronics, Beijing Institute of Technology, Beijing 100081, China)

Abstract: Passive synthetic aperture (PSA) positioning method can achieve high precision and resolution in passive location. However, existing approaches suffer from insufficient adaptability to non-ideal targets. In practical reconnaissance scenarios, complex pulse repetition interval (PRI) modulation and periodic beam scanning of radar emitters inevitably degrade PSA positioning performance. Specifically, periodic scanning causes block sparse observations and grating lobes, while nonuniform PRI disrupts phase coherence across the synthetic aperture, resulting in spectral leakage and elevated sidelobes. By exploiting the approximate linear frequency modulation (LFM) characteristic and fractional-domain sparsity of Doppler signal under broadside and small squint conditions, a fractional-domain reconstruction method based on compressed sensing (CS) for PSA positioning is proposed. A nonuniform sensing matrix is constructed at the true sampling instants, and the full-aperture Doppler phase history is reconstructed via orthogonal matching pursuit (OMP) for coherent accumulation positioning. Simulations under uniform, stagger, and jitter PRI conditions demonstrate effective suppression of grating lobes and spurious peaks, together with improved image contrast and localization accuracy over conventional PSA positioning.

Keywords: passive synthetic aperture positioning; complex PRI; periodic scanning; compressed sensing

1 Introduction

Passive localization determines emitter position by processing intercepted signal without active transmission, offering advantages in stealth and long-range detection [1]. Conventional two-step methods based on direction of arrival (DOA), time difference of arrival (TDOA), and frequency difference of arrival (FDOA) suffer from error accumulation [2–4]. Passive synthetic aperture (PSA) positioning avoids this by directly exploiting the full aperture phase history of the received signal under a moving platform, which achieves higher localization accuracy and spatial resolution [5–8].

Conventional PSA positioning algorithms are mostly developed under the uniform continuous sampling assumption, whereas modern radars adopt periodic beam scanning and complex pulse repetition interval (PRI) modulation to achieve spatial coverage and electronic counter-counter measures (ECCM) capability [9, 10], causing the receiver to intercept intermittent and nonuniformly sampled pulses. This leads to elevated sidelobe floor, grating lobes, and degraded positioning performance under conventional PSA positioning [11, 12].

Direct interpolation methods [13] rely on local neighborhood fitting and degrade into unre-

Manuscript received Apr. 22, 2026; revised May 28, 2026; accepted May 29, 2026. The associate editor coordinating the review of this manuscript was Dr. Hao Huan. The work was supported in part by the Stable-Support Scientific Project of China Research Institute of Radiowave Propagation (No.A240404180).

✉ Corresponding author. Email: rantao@bit.edu.cn

DOI: 10.15918/j.jbit1004-0579.2026.030

liable extrapolation when inter-sample spacing exceeds the signal's characteristic variation scale under sparse reception. Adaptive spectral estimation followed by uniform resampling [14] introduces two-stage error accumulation, as sparse sampling causes spectral leakage in the estimation step that is further propagated into the spatial domain during resampling. The relative mean deviation non uniform fast Fourier transform (RMD NUFFT) method [15] handles stagger PRI through azimuth and range trajectory fitting, but relies on accurate prior estimates of PRI and Doppler parameters, which are difficult to obtain under severe pulse loss caused by scanning. The fractional Fourier transform (FrFT)-based compressive sensing method in [12] alleviates ghost targets induced by periodic sparsity, yet does not address the additional nonuniformity introduced by complex PRI modulation.

To address the coupled effects of periodic sparse reception and nonuniform sampling induced by complex PRI, this paper proposes a PSA positioning method based on fractional-domain sparse reconstruction. The main contributions are as follows: 1) a fractional-domain nonuniform sensing matrix is constructed at the true sampling instants by exploiting the sparsity of the Doppler phase history in the fractional Fourier domain, enabling compressed sensing reconstruction under uniform, stagger, and jitter PRI conditions; 2) a full aperture phase history reconstruction and coherent back-projection positioning scheme is proposed which outperforms conventional PSA in positioning accuracy and focusing capability.

2 Signal Modeling and Problem Formulation

2.1 Signal Model

A passive airborne platform moves with constant velocity v along the x axis at altitude H, with instantaneous position $\boldsymbol{P}_{\mathrm{r}}(t)=[x_{p_0}+vt, y_{p_0}, H]^{\mathrm{T}}$. A stationary emitter is located at $\boldsymbol{P}_{\mathrm{s}}=[x_{\mathrm{s}}, y_{\mathrm{s}}, 0]^{\mathrm{T}}$. The slant range between the receiver and the emitter is

$$R(t)=\left\|\boldsymbol{P}_{\mathrm{r}}(t)-\boldsymbol{P}_{\mathrm{s}}\right\|_2 \tag{1}$$

As shown in Fig. 1, periodic beam scanning restricts signal reception to dwell windows of duration T_{dwell} within each scan cycle T_{scan}. Let τ_0 denote the start time of the first dwell window and Q the number of complete scan cycles within the total observation interval. The periodic scanning window can be expressed as

$$m(t)=\sum_{q=0}^{Q-1}\operatorname{rect}\left(\frac{t-\tau_0-qT_{\mathrm{scan}}-T_{\mathrm{dwell}}/2}{T_{\mathrm{dwell}}}\right) \tag{2}$$

where $\operatorname{rect}(x)$ denotes the rectangular window function, defined as

$$\operatorname{rect}(x)=\begin{cases}1 & |x|\leqslant 1/2\\ 0 & \text{otherwise}\end{cases} \tag{3}$$

Let the mean PRI be T_{r}, and let Δ_n denote the PRI offset of the nth pulse. The actual arrival time of the nth transmitted pulse is

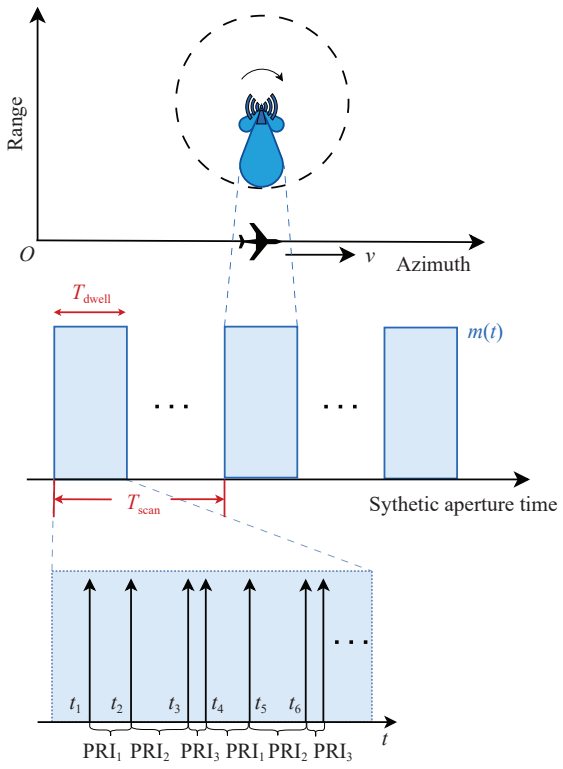


Fig. 1 Schematic of received signal

$$t_n = nT_{\mathrm{r}} + \delta_n, \quad \delta_n = \sum_{i=0}^{n-1} \Delta_i \tag{4}$$

where $n = 0, 1, \cdots, N_{\mathrm{p}} - 1$ and N_{p} denotes the pulse number within the complete aperture time. For uniform PRI, $\Delta_n = 0$; for stagger PRI, Δ_n follows a deterministic periodic pattern; and for jitter PRI, Δ_n is a zero-mean random variable.

Equivalently, let $\phi_n = \mathrm{mod}(t_n - \tau_0, T_{\mathrm{scan}})$. Then the discrete scanning indicator can be written as

$$m_n = m(t_n) = \begin{cases} 1 & \phi_n \in [0, T_{\mathrm{dwell}}] \\ 0 & \text{otherwise} \end{cases} \tag{5}$$

Thus, $m_n = 1$ indicates that the nth pulse falls within a dwell window and is effectively received, whereas $m_n = 0$ indicates that the pulse is missed because of periodic beam scanning. The valid pulse index set is defined as $\Omega = \{n \mid m_n = 1\}$, and the number of actually received pulses after pulse missing is $M = |\Omega| = \sum_{n=0}^{N_{\mathrm{p}}-1} m_n$.

The gated received pulse sequence can therefore be written as

$$y_n = m_n s_{\mathrm{r}}(t_n) + w_n \tag{6}$$

where $s_{\mathrm{r}}(t_n)$ denotes the ideal Doppler signal sampled at the nonuniform pulse arrival time t_n, and w_n denotes complex Gaussian noise.

2.2 Impact of Complex PRI and Periodic Scanning

Complex PRI displaces pulse arrival time from the uniform grid, which distorts the ideal Doppler spectrum. Specifically

$$Y_{\mathrm{PRI}}(f) = \sum_{n \in \Omega} \exp[-\mathrm{j}2\pi(f - f_{\mathrm{d}})nT_{\mathrm{r}}] \times \exp[-\mathrm{j}2\pi(f - f_{\mathrm{d}})\delta_n] \tag{7}$$

where $a_n(f) = \exp[-\mathrm{j}2\pi(f - f_{\mathrm{d}})\delta_n]$ represents the impact of complex PRI modulation. For stagger PRI, the periodicity of $a_n(f)$ gives rise to discrete parasitic spectral lines. For jitter PRI, the randomness of $a_n(f)$ weakens coherent accumulation and raises the sidelobe floor.

Periodic scanning further convolves the Doppler spectrum with a comb function spaced at $1/T_{\mathrm{scan}}$

$$Y(f) = \sum_{l=-\infty}^{\infty} c_l \, Y_{\mathrm{PRI}}\left(f - \frac{l}{T_{\mathrm{scan}}}\right) \tag{8}$$

where c_l denotes the amplitude coefficients.

As illustrated in Fig. 2, periodic scanning results in the translation of both the true Doppler component and the PRI induced spectral artifacts to the corresponding grating lobe locations.

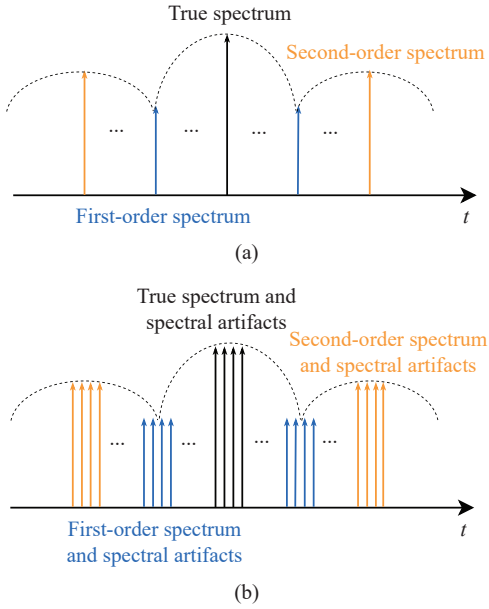


Fig. 2 Spectrum diagram of a third-order stagger PRI signal: (a) continuous aperture; (b) block sparse aperture

2.3 Fractional-Domain Sparsity of Ideal Doppler Signal

Let t_{c} denote the aperture center time, and define the reference slant range as $R_{\mathrm{c}} = R(t_{\mathrm{c}})$. The slant range curvature is significant and the corresponding quadratic phase is non-negligible when the emitter is in near field. Therefore, the slant range in Eq. (1) can be approximated by a Taylor polynomial expansion as

$$R(t) \approx R_{\mathrm{c}} + R'(t_{\mathrm{c}})(t - t_{\mathrm{c}}) + \frac{R''(t_{\mathrm{c}})}{2}(t - t_{\mathrm{c}})^2 = R_{\mathrm{c}} - v\sin\theta_{\mathrm{c}}(t - t_{\mathrm{c}}) + \frac{v^2\cos^2\theta_{\mathrm{c}}}{2R_{\mathrm{c}}}(t - t_{\mathrm{c}})^2 \tag{9}$$

where the squint angle θ_{c} satisfies $\sin\theta_{\mathrm{c}} = \dfrac{x_{\mathrm{s}} - x_{p0}}{R_{\mathrm{c}}}$ and $\cos^2\theta_{\mathrm{c}} = \dfrac{(y_{p0} - y_{\mathrm{s}})^2 + H^2}{R_{\mathrm{c}}^2}$.

Let $\tau = t - t_c$, where $\tau \in \left[-\frac{T_{sa}}{2}, \frac{T_{sa}}{2}\right]$. The ideal Doppler signal can be approximated as an LFM (linear frequency modulation) signal

$$s_r(\tau) = \beta_c \exp\left(\mathrm{j}2\pi f_d \tau - \mathrm{j}\pi\kappa\tau^2\right) \tag{10}$$

where $\beta_c = \beta \exp\left(-\mathrm{j}2\pi f_c R_c / c\right)$. The Doppler center frequency and chirp rate are defined as

$$f_d = -\frac{v \sin\theta_c}{\lambda} \tag{11}$$

$$\kappa = \frac{v^2 \cos^2\theta_c}{\lambda R_c} \tag{12}$$

For a LFM signal, the fractional Fourier transform of Eq. (10) at the optimal rotation angle $\alpha_0 = \operatorname{arccot}(2\pi\kappa)$ yields a dominant peak [16]

$$S_{\alpha_0}(u) \approx A\,\mathrm{sinc}\left(T_{sa}\left(u \csc\alpha_0 - f_d\right)\right) \tag{13}$$

where A is an amplitude constant. Eq. (13) indicates that the Doppler signal of a single emitter is highly concentrated in the optimal fractional domain as shown in Fig. 3.

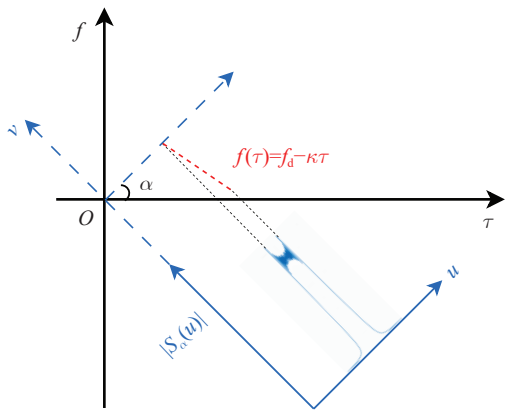


Fig. 3 Time-frequency projection of FrFT

3 Proposed Positioning Algorithm

3.1 Compressed Sensing Matrix Construction

To represent the nonuniform observations within a compressed sensing framework, the full-aperture Doppler phase history is represented over a fractional-domain CS dictionary composed of LFM atoms defined over a uniform frequency grid of N points. The sensing matrix is constructed using the actual sampling instants, enabling sparse recovery of fractional-domain coefficients from the $M \ll N$ available measurements. The uniform frequency grid is defined as

$$f_q = \frac{q - 1 - \lfloor N/2 \rfloor}{T_{sa}}, q = 1, 2, \cdots, N \tag{14}$$

where T_{sa} denotes the total synthetic aperture time and N is the number of grid points used to represent the complete aperture.

For a candidate chirp rate κ, define the continuous-time quadratic phase atom associated with the qth grid point as

$$\phi_q(t;\kappa) = \frac{1}{N}\exp(\mathrm{j}2\pi f_q t - \mathrm{j}\pi\kappa t^2) \tag{15}$$

Sampling Eq. (15) on $\boldsymbol{t}_\Omega$ yields the qth atom

$$\boldsymbol{\psi}_q(\kappa) = \frac{1}{N}\begin{bmatrix} \mathrm{e}^{\mathrm{j}2\pi f_q t_1 - \mathrm{j}\pi\kappa t_1^2} \\ \mathrm{e}^{\mathrm{j}2\pi f_q t_2 - \mathrm{j}\pi\kappa t_2^2} \\ \vdots \\ \mathrm{e}^{\mathrm{j}2\pi f_q t_M - \mathrm{j}\pi\kappa t_M^2} \end{bmatrix} \tag{16}$$

Stacking all atoms in columns, the Sensing matrix can be written as

$$\begin{aligned} \boldsymbol{\Psi}_\Omega(\kappa) = &\left[\boldsymbol{\psi}_1(\kappa), \cdots, \boldsymbol{\psi}_N(\kappa)\right] = \\ &\frac{1}{N}\exp(\mathrm{j}2\pi\boldsymbol{t}_\Omega\boldsymbol{f}^{\mathrm{T}}) \odot \exp(-\mathrm{j}\pi\kappa\,\boldsymbol{t}_\Omega^2\boldsymbol{e}_N^{\mathrm{T}}), \end{aligned} \tag{17}$$

where $\boldsymbol{f} = [f_1, f_2, \cdots, f_N]^{\mathrm{T}}$, $\boldsymbol{t}_\Omega = [t_1, t_2, \cdots, t_M]^{\mathrm{T}}$, $\odot$ denotes the Hadamard product, and $\boldsymbol{e}_N$ is the all-one vector of length N.

As illustrated in Fig. 4, the observation model can be written as

$$\boldsymbol{y}_\Omega = \boldsymbol{\Psi}_\Omega(\kappa)\boldsymbol{\theta} + \boldsymbol{w} \tag{18}$$

where $\boldsymbol{\theta} \in \mathbb{C}^{N\times 1}$ is the fractional-domain coefficient vector and $\boldsymbol{w}$ denotes the noise vector.

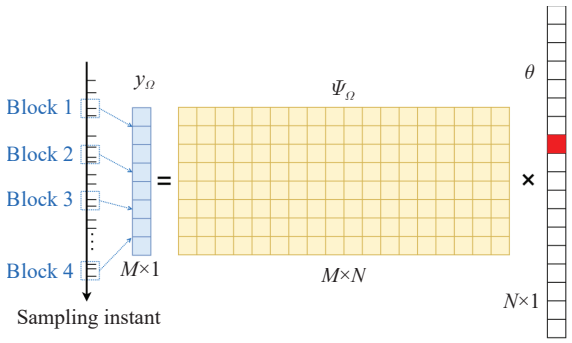


Fig. 4 Compressed sensing matrix

To further evaluate the influence of fractional-domain sparsity and pulse number on reconstruction reliability, the reconstruction success probability is defined as

$$P_{\text{succ}} = \frac{1}{N_{\text{MC}}} \sum_{q=1}^{N_{\text{MC}}} \mathbf{1}\left(\frac{\left\| \hat{\boldsymbol{\theta}}^{(q)} - \boldsymbol{\theta}^{(q)} \right\|_2^2}{\left\| \boldsymbol{\theta}^{(q)} \right\|_2^2} < \eta \right) \tag{19}$$

where N_{MC} is the number of Monte Carlo trials, η is the reconstruction error threshold, $\boldsymbol{\theta}^{(q)}$ is the true fractional-domain coefficient vector in the qth trial, and $\hat{\boldsymbol{\theta}}^{(q)}$ is the corresponding reconstructed coefficient vector. For example, $\eta = 10^{-2}$ means that the normalized reconstruction error energy is lower than 1%, corresponding to -20 dB.

As shown in Fig. 5, the reconstruction success probability increases with increasing pulse interception ratio $\rho = M/N_{\text{p}}$ and decreasing sparsity level K_θ. This is because a larger number of intercepted pulses provides more sufficient observation information, making OMP more reliable in selecting the correct support set. In contrast, a larger K_θ means that more nonzero fractional-domain components need to be recovered, which increases the probability of atom misselection and reduces the reconstruction success probability.

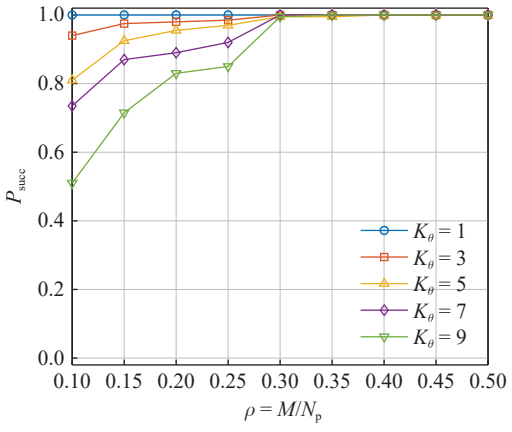


Fig. 5 Reconstruction success probability

3.2 Passive Synthetic Aperture Positioning

The chirp rate κ is estimated by maximizing the atom response over a candidate set $\mathcal{K}$

$$\hat{\kappa} = \arg\max_{\kappa \in \mathcal{K}} \max_{1 \leqslant q \leqslant N} \left| \psi_q^{\text{H}}(\kappa) \boldsymbol{y}_\Omega \right| \tag{20}$$

With $\hat{\kappa}$ fixed, the received signal is represented by Eq. (18). Since the ideal Doppler signal can be approximated as an LFM signal, only a few dominant atoms contribute significantly to the representation Eq. (17) in the optimal fractional domain. Therefore, the coefficient vector $\boldsymbol{\theta}$ can be estimated through sparse approximation as

$$\begin{aligned} \hat{\boldsymbol{\theta}} &= \arg\min \|\boldsymbol{\theta}\|_1 \\ &\text{s.t.} \quad \left\| \boldsymbol{y}_\Omega - \boldsymbol{\Psi}_\Omega(\hat{\kappa}) \boldsymbol{\theta} \right\|_2^2 \leqslant \varepsilon \end{aligned} \tag{21}$$

where ε denotes the reconstruction error tolerance. Eq. (21) can be solved by OMP, which iteratively selects the dominant atom with the maximum response and estimates its coefficient [17].

After obtaining the dominant fractional-domain atoms and their coefficients, the full-aperture signal is synthesized on the dense uniform grid $\{\bar{\tau}_n\}_{n=1}^N$ by

$$\hat{\boldsymbol{y}}_{\text{full}} = \boldsymbol{\Phi}(\hat{\kappa}) \hat{\boldsymbol{\theta}} \tag{22}$$

where $\boldsymbol{\Phi}(\hat{\kappa}) \in \mathbb{C}^{N \times N}$ is the synthesis dictionary defined on the dense uniform grid. Its qth atom is given by

$$\boldsymbol{\Phi}_q(\hat{\kappa}) = \frac{1}{N} \begin{bmatrix} \mathrm{e}^{\mathrm{j}2\pi f_q \bar{\tau}_1 - \mathrm{j}\pi\hat{\kappa}\bar{\tau}_1^2} \\ \mathrm{e}^{\mathrm{j}2\pi f_q \bar{\tau}_2 - \mathrm{j}\pi\hat{\kappa}\bar{\tau}_2^2} \\ \vdots \\ \mathrm{e}^{\mathrm{j}2\pi f_q \bar{\tau}_N - \mathrm{j}\pi\hat{\kappa}\bar{\tau}_N^2} \end{bmatrix} \tag{23}$$

where $\bar{\boldsymbol{\tau}}^{(2)} = [\bar{\tau}_1^2, \bar{\tau}_2^2, \ldots, \bar{\tau}_N^2]^{\text{T}}$.

As shown in Fig. 6, for a candidate ground position $\boldsymbol{P}$, define the reference phase vector

$$\boldsymbol{s}_{\text{ref}}(\boldsymbol{P}) = \begin{bmatrix} \exp\left(-\mathrm{j}\dfrac{2\pi}{\lambda} R(\bar{\tau}_1; \boldsymbol{P}) \right) \\ \exp\left(-\mathrm{j}\dfrac{2\pi}{\lambda} R(\bar{\tau}_2; \boldsymbol{P}) \right) \\ \vdots \\ \exp\left(-\mathrm{j}\dfrac{2\pi}{\lambda} R(\bar{\tau}_N; \boldsymbol{P}) \right) \end{bmatrix} \tag{24}$$

where $R(\bar{\tau}_n; \boldsymbol{P})$ denotes the geometric distance between the platform position and the candidate location $\boldsymbol{P}$ at slow time $\bar{\tau}_n$. The emitter position is estimated by

$$\hat{\boldsymbol{P}} = \arg\max_{\boldsymbol{P} \in \Omega_p} \left| \boldsymbol{s}_{\text{ref}}^{\text{H}}(\boldsymbol{P}) \hat{y}_{\text{full}} \right|^2 \tag{25}$$

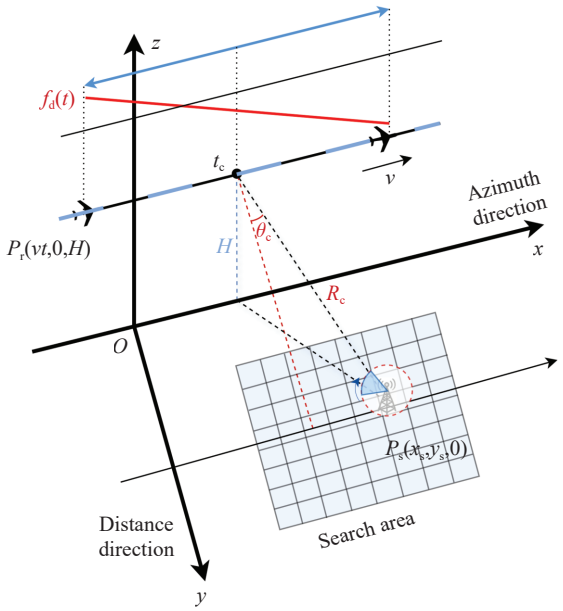


Fig. 6 PSA positioning scenario

where Ω_p denotes the search region. The complete procedure is summarized in Algorithm 1.

Algorithm 1 CS-based PSA positioning method

Require: intercepted signal $\boldsymbol{y}_\Omega$; sampling instants $\boldsymbol{t}_\Omega$; chirp rate set $\mathcal{K}$; error tolerance ε; uniform grid size N; search region Ω_p

Ensure: estimated position $\hat{\boldsymbol{P}}$

1: generate frequency grid $\boldsymbol{f}_q$ via (14)

2: **for** each $\kappa \in \mathcal{K}$ **do**

3: build sensing matrix $\boldsymbol{\Psi}_\Omega(\kappa)$ via (17)

4: compute $C(\kappa) = \max_q \left|\boldsymbol{\psi}_q^{\mathrm{H}} \boldsymbol{y}_\Omega\right|$

5: **end for**

6: estimate $\hat{\kappa} = \arg\max_\kappa C(\kappa)$ via (20)

7: solve (21) by OMP to obtain $\hat{\boldsymbol{\theta}}$

8: construct uniform synthesis dictionary $\boldsymbol{\Phi}(\hat{\kappa})$

9: compute $\hat{\boldsymbol{y}}_{\text{full}} = \boldsymbol{\Phi}(\hat{\kappa})\hat{\boldsymbol{\theta}}$ via (22)

10: **for** each $\boldsymbol{P} \in \Omega_p$ **do**

11: generate reference phase $\boldsymbol{s}_{\text{ref}}(\boldsymbol{P})$ via (24)

12: compute $J(\boldsymbol{P}) = \left|\boldsymbol{s}_{\text{ref}}^{\mathrm{H}}(\boldsymbol{P})\hat{\boldsymbol{y}}_{\text{full}}\right|^2$

13: **end for**

14: **return** $\hat{\boldsymbol{P}} = \arg\max_{\boldsymbol{P}\in\Omega_p} J(\boldsymbol{P})$ via (25)

3.3 Computational Complexity

Let $K = |\mathcal{K}|$ the number of candidate chirp rates, S the sparsity level or the number of OMP iterations, and $G = |\Omega_p|$ the number of spatial search grids. The chirp-rate search requires approximately $\mathcal{O}(KMN)$ operations for computing atom responses over all candidates. After $\hat{\kappa}$ is determined, the OMP-based sparse recovery has a complexity of approximately $\mathcal{O}(SMN)$ when $S \ll N$. The full-aperture synthesis using the selected atoms requires $\mathcal{O}(SN)$ operations, and the final PSA image formation requires $\mathcal{O}(GN)$ operations. Therefore, the overall computational complexity is approximately

$$\mathcal{O}(KMN + SMN + SN + GN) \tag{26}$$

The dominant terms are the chirp-rate search and the spatial coherent accumulation. The complexity can be further reduced by using a coarse-to-fine spatial search strategy.

4 Simulation Results

To verify the proposed method, simulations are conducted for a single emitter scenario with a uniformly moving receiver. The emitter operates at 9.41 GHz (X-band) in a periodic scanning mode, and the receiver intercepts pulses only within the beam dwell interval of each scan cycle. Three PRI modulation modes, including uniform PRI, stagger PRI, and jitter PRI, are considered to evaluate the adaptability of the proposed method to complex PRI modulation. The simulation parameters are listed in Tab. 1.

Fig. 7 presents the positioning results of con-

Tab. 1 Simulation parameters

Parameters	Value
Carrier freq. (GHz)	9.41
Platform speed (m/s)	100
Platform height (km)	10
Synthetic time (s)	10
PRI T_r (ms)	3
Staggered PRI	$[0.5 : 1.0 : 1.5]T_r$
Jittered PRI	$(1 \pm 30\%)T_r$
Scan cycle T_{scan} (s)	2.5
Beam dwell time T_{dwell} (s)	1.25
Target $\boldsymbol{P}_s$ (km)	(0, 80)

ventional PSA positioning and proposed method. Stagger PRI produces parasitic position peaks consistent with the theoretical prediction at 2 856 m and its multiples, as shown in Fig. 7(b). The result for jitter PRI in Fig. 7(c) exhibits an elevated background level. The grating lobe positions caused by periodic scanning in Fig. 7(d) approximately match the theoretical prediction $\Delta x = \lambda R_c / v T_{\text{scan}} \approx 17.13$ m.

Fig. 8 presents the positioning results after reconstruction by the proposed method. Both grating lobes and spurious peaks are effectively suppressed, and the final positioning image exhibits a well focused single peak.

Define the image contrast (IC) and peak sidelobe ratio (PSLR) as [18, 19]

$$\text{IC} = \frac{\sqrt{\dfrac{1}{N_{\Omega_p}} \sum\limits_{\boldsymbol{P} \in \Omega_p} \left(J(\boldsymbol{P}) - \bar{J} \right)^2}}{\bar{J}} \tag{27}$$

$$\text{PSLR} = 10 \lg \left(\frac{\max\limits_{\boldsymbol{P} \notin \Omega_{\hat{\boldsymbol{P}}}} J(\boldsymbol{P})}{J\left(\hat{\boldsymbol{P}}\right)} \right) \tag{28}$$

where N_{Ω_p} is the number of grid points in the search region, and $\bar{J}$ denotes the mean of the cost function. $\Omega(\hat{\boldsymbol{P}}) = \{\hat{\boldsymbol{P}} = (x, y) \mid |x - x_{\hat{\boldsymbol{P}}}| \leqslant w_x, |y - y_{\hat{\boldsymbol{P}}}| \leqslant w_y\}$ denotes the main lobe protection window centered at $\hat{\boldsymbol{P}}$, where w_x and w_y represent the width of main lobe in azimuth and range, respectively.

To quantitatively compare the focusing performance of the conventional PSA positioning and the proposed method, the IC and PSLR values for discontinuous radar signal under uniform, stagger, and jitter PRI are listed in Tab. 2.

Monte Carlo simulations are conducted to compare the positioning performance of the proposed method and conventional PSA positioning under varying SNR, as shown in Fig. 9. By reconstructing the full aperture signal, the proposed method achieves smaller positioning error than conventional PSA positioning, especially in the low SNR region.

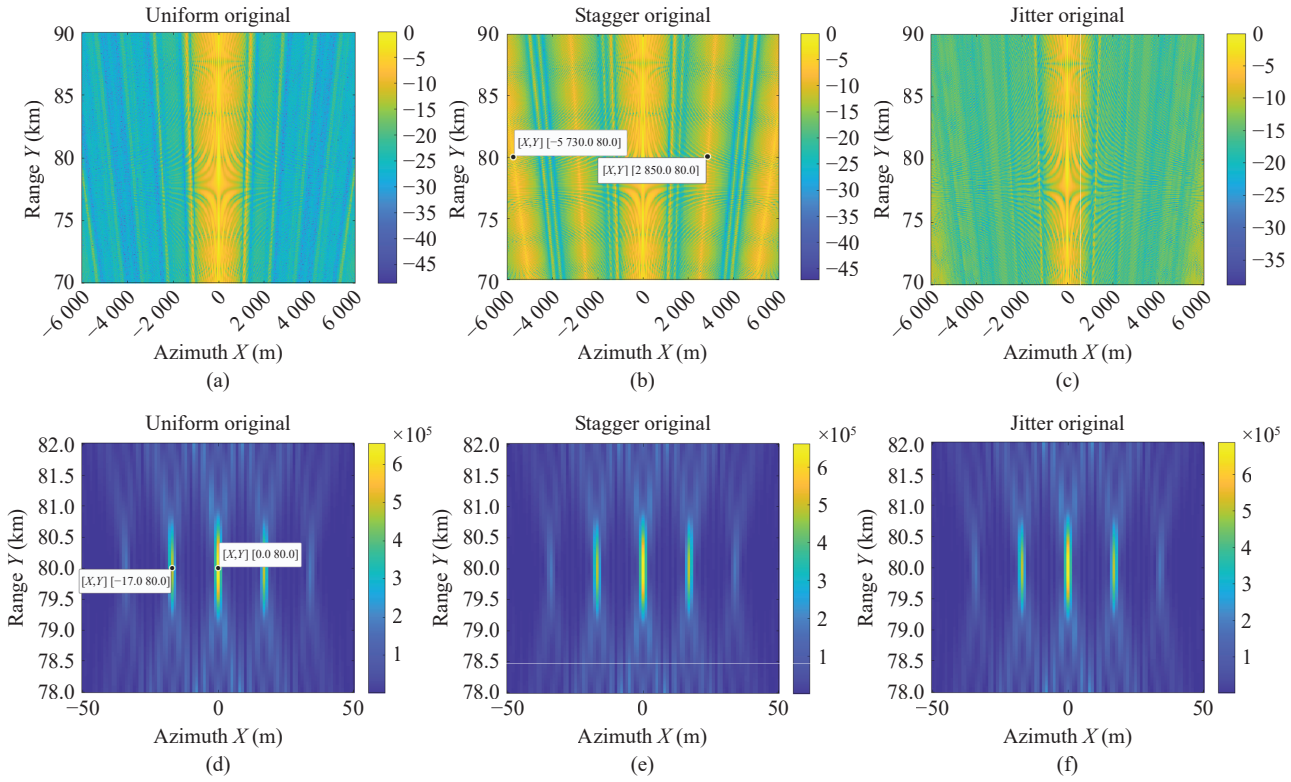


Fig. 7 Positioning images before reconstruction: (a)–(c) coarse search results; (d)–(f) fine search results

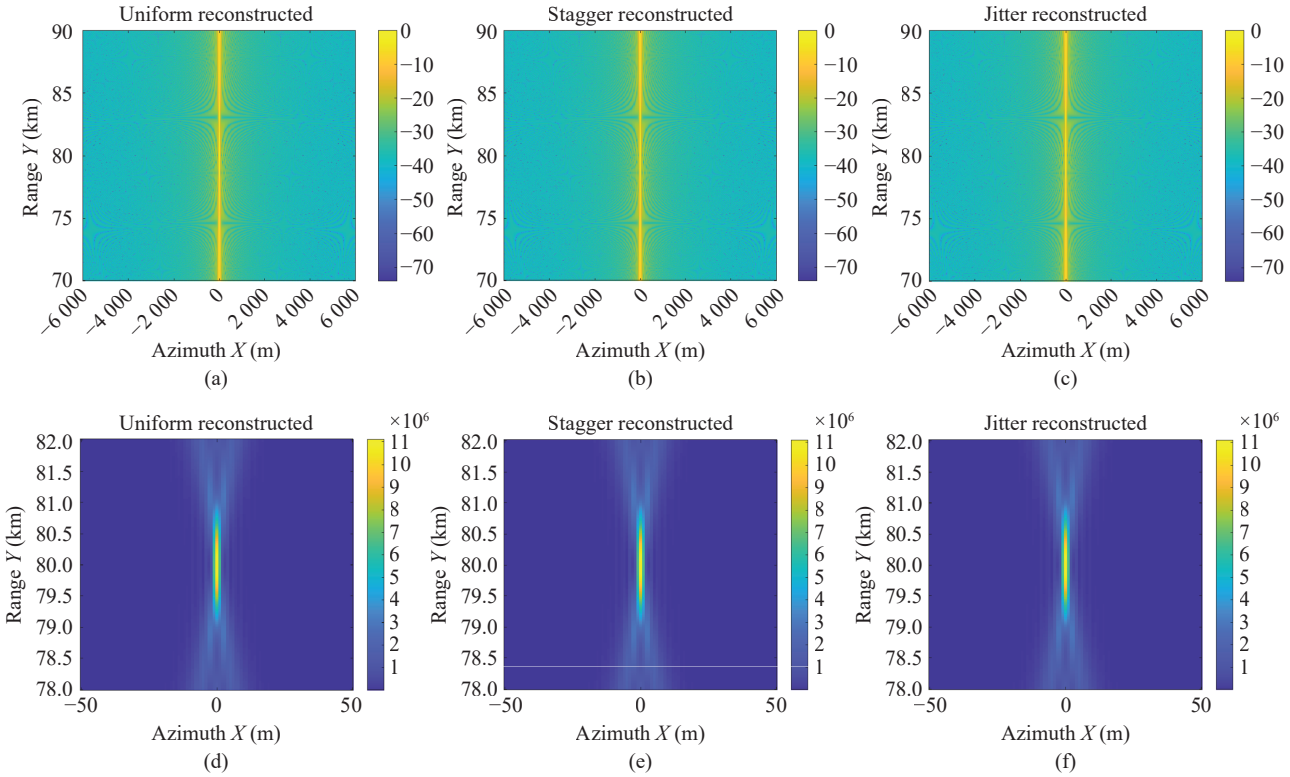


Fig. 8 Positioning images after reconstruction: (a)–(c) coarse search results; (d)–(f) fine search results

Tab. 2 Focusing quality comparison

Method	Indicators	Conventional	Proposed
Uniform	IC	0.8532	3.1998
	PSLR (dB)	-0.0831	-3.5316
Stagger	IC	0.8629	3.1998
	PSLR (dB)	-0.0464	-3.5336
Jitter	IC	0.9572	3.1684
	PSLR (dB)	-0.0004	-3.5146

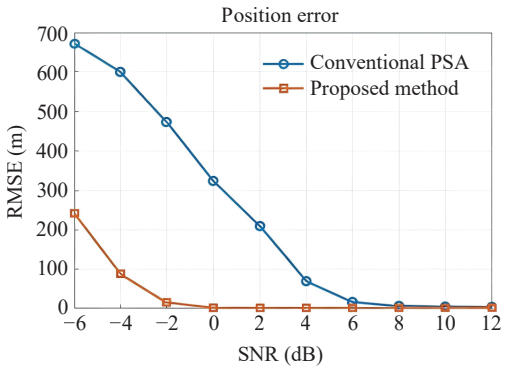


Fig. 9 Positioning RMSE versus SNR

5 Conclusion

This paper presents a passive synthetic aperture localization method based on optimal fractional-domain dominant atoms extraction and matching. By constructing a nonuniform compressed-sensing dictionary at the actual sampling instants, the proposed method achieves coherent full-aperture phase-history reconstruction under periodic beam scanning and nonuniform PRI modulation. Simulation results demonstrate that it effectively improves focusing quality and localization accuracy, and outperforms conventional PSA positioning in robustness under uniform, stagger, and jitter PRI conditions. This work focuses on the single-emitter case to validate the proposed full-aperture phase-history reconstruction under complex PRI modulation and periodic scanning. Multi-emitter positioning, which involves additional challenges such as time-frequency aliasing and target association, remains a direction for future investigation.

References:

[1] R. Zekavat and R. M. Buehrer, *Source localization: Algorithms and analysis*. Hoboken, NJ, USA: Wiley, 2012.

[2] R. Schmidt,"Multiple emitter location and signal parameter estimation," *IEEE Transactions on*

Antennas and Propagation, vol. 34, no. 3, pp. 276-280, 1986.

[3] Y. Huang, J. Benesty, G. W. Elko, and R. M. Mersereati,"Real-time passive source localization: a practical linear-correction least-squares approach," *IEEE Transactions on Speech and Audio Processing*, vol. 9, no. 8, pp. 943-956, 2001.

[4] K. C. Ho, X. Lu, and L. Kovavisaruch,"Source localization using TDOA and FDOA measurements in the presence of receiver location errors: Analysis and solution," *IEEE Transactions on Signal Processing*, vol. 55, no. 2, pp. 684-696, 2007.

[5] A. Li, H. Huan, R. Tao, and L. Zhang,"Passive synthetic aperture high-precision radiation source location by single satellite," *IEEE Geoscience and Remote Sensing Letters*, vol. 19, pp. 1-5, 2022.

[6] Y. Wang, G. C. Sun, Y. Wang, Z. Zhang, M. Xing, and X. Yang,"A high-resolution and high-precision passive positioning system based on synthetic aperture technique," *IEEE Transactions on Geoscience and Remote Sensing*, vol. 60, pp. 1-13, 2022.

[7] L. Zhang, H. Huan, R. Tao, and Y. Wang,"Emitter localization algorithm based on passive synthetic aperture," *IEEE Transactions on Aerospace and Electronic Systems*, vol. 58, no. 4, pp. 2687-2701, 2022.

[8] J. Yang, H. Huan, and R. Tao,"Multisubaperture backward projection positioning algorithm for radiation sources by single satellite," *IEEE Transactions on Aerospace and Electronic Systems*, vol. 61, no. 2, pp. 1267-1282, 2025.

[9] H. Hmam,"Scan-based emitter passive localization," *IEEE Transactions on Aerospace and Electronic Systems*, vol. 43, no. 1, pp. 36-54, 2007.

[10] M. I. Skolnik, *Introduction to radar systems*, 3 rd ed. New York: McGraw-Hill, 2001.

[11] J. Zhu, T. Zhao, T. Huang, and D. Zhang, "Analysis of random pulse repetition interval radar, " in *Proceedings of 2016 IEEE Radar Conference (RadarConf)*, Philadelphia, PA, USA, pp. 1-5, 2016.

[12] J. Sun, H. Huan, R. Tao, and Y. Wang,"A passive synthetic aperture localization method based on sparse sampling reconstruction," *IEEE Geoscience and Remote Sensing Letters*, vol. 22, pp. 1-5, 2025.

[13] J. A. Fessler and B. P. Sutton,"Nonuniform fast fourier transforms using min-max interpolation," *IEEE Transactions on Signal Processing*, vol. 51, no. 2, pp. 560-574, 2003.

[14] X. Wang, R. Wang, Y. Deng, W. Wang, and N. Li,"SAR signal recovery and reconstruction in staggered mode with low oversampling factors," *IEEE Geoscience and Remote Sensing Letters*, vol. 15, no. 5, pp. 704-708, 2018.

[15] L. Zhang, H. Huan, R. Tao, and Y. Wang,"Passive localization algorithm for PRI-staggered radar signal based on RMD and NUFFT," *IEEE Sensors Journal*, vol. 24, no. 7, pp. 10 755-10768, 2024.

[16] A. I. Zayed,"A convolution and product theorem for the fractional fourier transform," *IEEE Signal Processing Letters*, vol. 5, no. 4, pp. 101-103, 1998.

[17] J. A. Tropp and A. C. Gilbert,"Signal recovery from random measurements via orthogonal matching pursuit," *IEEE Transactions on Information Theory*, vol. 53, no. 12, pp. 4655-4666, 2007.

[18] S. Zhang, M. Xing, R. Guo, L. Zhang, and Z. Bao,"Interference suppression algorithm for SAR based on time-frequency transform," *IEEE Transactions on Geoscience and Remote Sensing*, vol. 49, no. 10, pp. 3765-3779, 2011.

[19] C. Hu, Y. Li, X. Dong, R. Wang, and D. Ao,"Performance analysis of L-band geosynchronous SAR imaging in the presence of ionospheric scintillation," *IEEE Transactions on Geoscience and Remote Sensing*, vol. 55, no. 1, pp. 159-172, 2017.



Huanhuan Li received the B.E. degree in electronic information science and technology from Southwest Jiaotong University, Chengdu, China, in 2023. She is currently pursuing the M.E. degree in information and communication engineering at Beijing Institute of Technology, Beijing, China.



Ran Tao received the B.S. degree in radar engineering from Electronic Engineering Institute of PLA, Hefei, China, in 1985, and the M.S. and Ph.D. degrees in communication and electronic systems and electromagnetic measurement technology and instrument from Harbin Institute of Technology, Harbin, China, in 1990 and 1993, respectively. In 2001, he was a Senior Visiting Scholar with the University of Michigan, Ann Arbor, MI, USA. He is currently a professor with the School of Information and Electronics, Beijing Institute of Technology, Beijing, China. He has authored or coauthored three books and more than 100 peer reviewed journal articles. His current research interests include the fractional Fourier transform and its applications, as well as radar and communication systems.